Int. J. Heat Mass Transfer. Vol. 36, No. 14, pp. 3593–3602, 1993
Printed in Great Britain

0017–9310/93 $6.00+0.00

Free convection from an elliptic cylinder with major axis vertical

H. M. BADR and K. SHAMSHER
Mechanical Engineering Department, King Fahd University of Petroleum & Minerals, Dhahran 31261, Saudi Arabia

(*Received* 23 *July* 1992)

Abstract—The problem of free convection heat transfer from a horizontal elliptic cylinder placed with its major axis vertical in a fluid of infinite extent is investigated. The investigation is based on the solution of the conservation equations of mass, momentum, and energy. The problem is solved for Rayleigh numbers ranging from 10 to 1000 and for a constant value of Prandtl number ($Pr = 0.7$). The cylinder axis ratio (minor to major) varies from 0.1 to 0.964 approaching a flat plate at one end and a circular cylinder at the other. Results are presented for the local and average Nusselt numbers along with details of the thermal and velocity fields given in the form of isotherm and streamline patterns. The method of solution is validated by comparing results with the available theoretical and experimental data for the circular cylinder and the flat plate as limiting cases.

1. INTRODUCTION

NATURAL convection heat transfer has gained considerable attention because of its numerous applications in the areas of energy conservation, cooling of electrical and electronic components, design of solar collectors, heat exchangers, and many others. The main difficulty in solving natural convection problems lies in the determination of the velocity field which greatly influences the heat transfer process.

The increasing interest in developing compact and highly efficient heat exchangers motivated researchers to study heat transfer from tubes of non-circular cross-section. Special attention was focused on tubes of elliptic cross-section since they were found to create less resistance to the cooling fluid which results in less pumping power. Although forced convection is dominant in heat exchangers, natural convection becomes the only mode of heat transfer in case of power failure. Natural convection from an inclined tube of circular cross-section is actually a direct application of the present study since the tube cross-section in direction of the buoyancy driven flow becomes elliptic in shape. Moreover, the elliptic tube geometry is flexible enough to approach a circular tube when the axis ratio approaches unity and to approach a flat plate when the axis ratio is very small.

Research on natural convection from cylinders was mostly focused on horizontal circular cylinders. McAdams [1] compiled the data of natural convection flow over a horizontal circular cylinder obtained by a number of workers prior to 1952. He also recommended correlations for a wide range of Rayleigh number. The boundary-layer equations were solved by Hermann [2], employing suitable transformations, for the case of uniform surface temperature. Chiang and Kay [3], using a similar procedure, solved the same problem for prescribed surface temperature and heat flux boundary conditions. Elliot [4] studied natural convection for two-dimensional or axisymmetric bodies following a sudden temperature increase. The study was based on a series solution at small times for the temperature and stream function. The theory was applied to a circular cylinder and the small time solution was extrapolated to predict the steady heat transfer coefficient. The extrapolation procedure failed near the top of the cylinder since the boundary-layer approximations were invalid in that region. The boundary-layer equations were also solved by Merkin [5] for the case of a horizontal isothermal cylinder. Comparison with previous experimental studies indicated that the approach is inapplicable near the top of the cylinder.

Experimental investigation of natural convection flow from a circular cylinder was carried out by Pera and Gebhart [6] who visualized the flow using granules of plastic and a laser light in water. They reported no boundary-layer separation, however, very irregular flow separation and reversal occurred near the middle and upper part of the surface during transient flow periods. The inapplicability of boundary-layer assumptions in the region of the plume even at high Ra values motivated some researchers to solve the full conservation equations. Kuehn and Goldstein [7] solved the problem assuming that the fluid leaves radially in the plume with negligible radial temperature gradient. The obtained results compared reasonably well with the experimental observations using a Mach–Zehnder interferometer. Farouk and Guceri [8] solved the same problem for the cases of non-uniform temperature and heat flux boundary conditions. Badr [9] solved the problem of transient natural convection from an isothermal circular cylinder which was heated either suddenly or gradually to a constant

NOMENCLATURE

a, b cylinder major and minor axes
f_n function defined in equation (10)
F_x, F_y x and y components of the body force
g gravitational acceleration
Gr Grashof number, $g\beta(T_s - T_\infty)b^3/\nu^2$
g_n function defined in equation (10)
h local heat transfer coefficient
$\bar{h}$ average heat transfer coefficient
H_0, H_n function defined in equation (10)
J Jacobian of transformation
k thermal conductivity
l focal distance
L elliptic section perimeter
Nu local Nusselt number
$\overline{Nu}$ average Nusselt number
Pr Prandtl number, ν/α
$\dot{q}$ rate of heat transfer per unit area
Ra Rayleigh number, $Gr\,Pr$
t time
u, v velocities in x and y direction, respectively
u_ξ, u_η velocities in ξ and η direction, respectively
x, y rectilinear coordinates.

Greek symbols
α thermal diffusivity
β coefficient of volumetric thermal expansion
ζ vorticity
η, ξ elliptical coordinates
ν kinematic viscosity
ρ density
ϕ dimensionless temperature
ψ stream function.

Subscripts
0 at the surface
∞ at infinite distance from the surface.

surface temperature. The Navier–Stokes and energy equations were solved in logarithmic polar coordinates which facilitated in virtually approaching infinity to satisfy the far field boundary conditions. Correlation studies were reported by Churchill and Chu [10] and Morgan [11].

Very few theoretical studies on natural convection from an elliptic cylinder have been published and no experimental work has been reported so far. Lin and Chao [12] replaced the buoyancy term in the boundary-layer equations by a hypothetical outer stream velocity function. Series solutions were obtained for two-dimensional and axisymmetric bodies with circular and elliptic cylinders as special cases. The solution had the drawback of its inapplicability in the buoyant plume region. Raithby and Hollands [13] solved the problem of free convection from an elliptic cylinder with major axis vertical. A thin layer analysis applicable to regions in which the boundary-layer is much thinner than the local radius of curvature was modified to take into account the effect of curvature. For the limiting cases of elliptical cylinder (the vertical flat plate and the horizontal circular cylinder), the average Nusselt numbers were found to be in good agreement with the experimental data for a wide range of Rayleigh numbers. Merkin [14], using a solution procedure similar to ref. [5], solved the boundary-layer equations for an elliptic cylinder with major axis either vertical or horizontal. Local and average heat transfer rates were calculated for the cases of either constant surface temperature or constant heat flux. The obtained results have the same drawback as discussed previously for the case of a circular cylinder [5].

The present work aims to solve the problem of natural convection heat transfer from an isothermally heated horizontal elliptical cylinder placed with its major axis vertical in a quiescent Boussinesq fluid of infinite extent. The study is based on the solution of the full conservation equations of mass, momentum and energy. The effect of cylinder axis ratio and Rayleigh number on the local and average heat transfer coefficients are investigated.

2. PROBLEM STATEMENT AND GOVERNING EQUATIONS

The problem considered is that of natural convection heat transfer from a horizontal cylinder of elliptic cross-section with a and b representing its major and minor axes respectively as shown in Fig. 1. The cylinder surface has a constant temperature T_s and is placed with its major axis vertical in a quiescent Boussinesq fluid of infinite extent. The fluid far away from the cylinder surface has a constant temperature T_∞. The flow in the neighbourhood of the cylinder surface is driven by buoyancy forces only and is assumed laminar. The cylinder is assumed to be long enough so that the end effects can be neglected and the flow is considered two-dimensional. Neglecting viscous dissipation and radiation heat transfer effects, the governing equations of motion and energy can be expressed in Cartesian coordinates as

$$\frac{\partial \zeta'}{\partial t'} = \nu \nabla^2 \zeta' - \frac{\partial \psi'}{\partial y}\frac{\partial \zeta'}{\partial x} + \frac{\partial \psi'}{\partial x}\frac{\partial \zeta'}{\partial y} + \frac{1}{\rho}\left(\frac{\partial F_y}{\partial x} + \frac{\partial F_x}{\partial y}\right) \tag{1}$$

$$\zeta' = -\nabla^2 \psi' \tag{2}$$

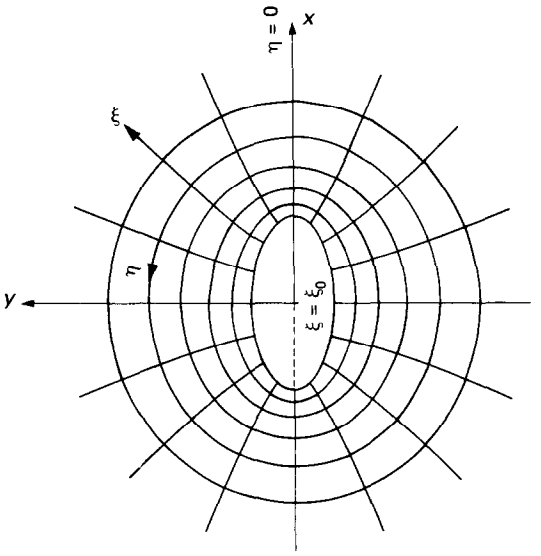

FIG. 1. The coordinate systems.

$$\frac{\partial T}{\partial t'} = \alpha\nabla^2 T - \frac{\partial \psi'}{\partial y}\frac{\partial T}{\partial x} + \frac{\partial \psi'}{\partial x}\frac{\partial T}{\partial y} \tag{3}$$

where ζ' is the vorticity, ψ' is the stream function, ν is the kinematic viscosity, ρ is the density, F_x and F_y are the x and y components of the body force, T is the temperature, α is the thermal diffusivity and t' is the time. In the present problem, the body force is mainly due to buoyancy and accordingly

$$F_x = \rho g\beta(T - T_\infty), \quad F_y = 0$$

where g is the gravitational acceleration and β is the coefficient of thermal expansion.

For convenience, the governing equations (1)–(3) are written in the elliptic coordinate system (ξ, η) using the transformation

$$x = l\cosh\xi\cos\eta, \quad y = l\sinh\xi\sin\eta$$

where l is the focal distance and $\eta = 0$ corresponds to the topmost point on the cylinder surface as shown in Fig. 1. The resulting equations were then normalized by using the following dimensionless variables:

$$\psi = \frac{\psi'}{\alpha}; \quad \zeta = \frac{\zeta' b^2}{\alpha}; \quad t = \frac{t'\alpha}{b^2}; \quad \phi = \frac{T - T_\infty}{T_s - T_\infty}.$$

The final equations become

$$J\frac{\partial \zeta}{\partial t} = Pr\left(\frac{\partial^2\zeta}{\partial\xi^2} + \frac{\partial^2\zeta}{\partial\eta^2}\right) - \frac{\partial\psi}{\partial\eta}\frac{\partial\zeta}{\partial\xi} + \frac{\partial\psi}{\partial\xi}\frac{\partial\zeta}{\partial\eta} - \frac{Pr\,Ra}{\lambda}\left(s_1\frac{\partial\phi}{\partial\eta} + s_2\frac{\partial\phi}{\partial\xi}\right) \tag{4}$$

where s_1 and s_2 are defined as:

$$s_1 = \sinh\xi\cos\eta \quad \text{and} \quad s_2 = \cosh\xi\sin\eta$$

$$J\zeta = -\left(\frac{\partial^2\psi}{\partial\xi^2} + \frac{\partial^2\psi}{\partial\eta^2}\right) \tag{5}$$

$$J\frac{\partial\phi}{\partial t} = \left(\frac{\partial^2\phi}{\partial\xi^2} + \frac{\partial^2\phi}{\partial\eta^2}\right) - \frac{\partial\psi}{\partial\eta}\frac{\partial\phi}{\partial\xi} + \frac{\partial\psi}{\partial\xi}\frac{\partial\phi}{\partial\eta} \tag{6}$$

where Pr $(= \nu/\alpha)$ is the Prandtl number, Ra $(= Pr\,g\beta(T_s - T_\infty)b^3/\nu^2)$ is the Rayleigh number, $\lambda = b/l$, and J is the Jacobian of transformation defined as

$$J = \frac{1}{2\lambda^2}(\cosh 2\xi - \cos 2\eta). \tag{7}$$

The dimensionless velocity components in the ξ and η directions are related to ψ by the equations

$$u_\xi = \frac{1}{J^{1/2}}\frac{\partial\psi}{\partial\eta} \quad \text{and} \quad u_\eta = -\frac{1}{J^{1/2}}\frac{\partial\psi}{\partial\xi}.$$

The boundary conditions for the velocity and thermal fields are

$$\psi = \frac{\partial\psi}{\partial\eta} = \frac{\partial\psi}{\partial\xi} = 0 \quad \text{and} \quad \phi = 1 \quad \text{at} \quad \xi = \xi_0$$

$$\psi, \quad \frac{\partial\psi}{\partial\eta}, \quad \frac{\partial\psi}{\partial\xi}, \quad \phi, \quad \zeta \to 0 \quad \text{as} \quad \xi \to \infty. \tag{8}$$

The conditions in equation (8) are based on the no-slip, impermeability and isothermal conditions at the cylinder surface and the ambient conditions far away.

In the present problem, the flow and thermal fields are symmetric about a vertical line coinciding with the major axis, herein after refered to as the line of symmetry. The following represents additional conditions along the line of symmetry

$$\frac{\partial\psi}{\partial\xi} = \zeta = \frac{\partial\phi}{\partial\eta} = \frac{\partial u_\xi}{\partial\eta} = 0 \quad \text{at} \quad \eta = 0 \quad \text{and} \quad \eta = \pi. \tag{9}$$

3. THE METHOD OF SOLUTION

The details of the steady velocity and thermal fields are obtained by studying the time-development of both fields when the surface temperature is suddenly increased from T_∞ to T_s. At the same moment, the fluid everywhere is at rest and has a uniform temperature T_∞. As a result of the surface temperature increase, the fluid adjacent to the cylinder is first heated by conduction and then starts to move upward driven by buoyancy force. With the increase of time, the velocity and thermal layers grow until eventually reaching a steady condition. The approach is, in principle, similar to that used by Badr [15] for studying laminar combined convection from a horizontal circular cylinder. Because of symmetry of the velocity and thermal fields about $\eta = 0$ and following ref. [15], one can express ψ, ζ and ϕ in the form

$$\psi = \sum_{n=1}^{N} f_n(\xi, t)\sin n\eta$$

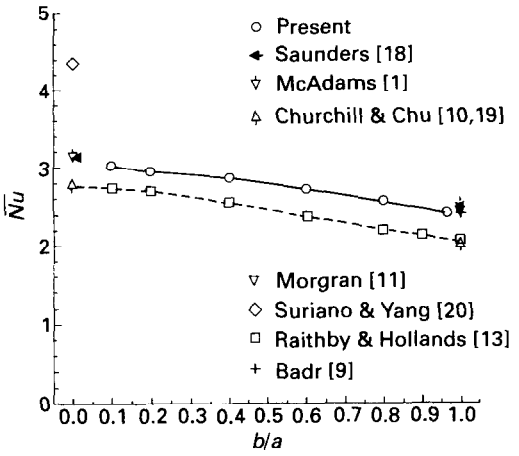

FIG. 2. Comparison of average Nusselt number for different axis ratios with previous theoretical and experimental results for the case of $Ra = 300$.

$$\zeta = \sum_{n=1}^{N} g_n(\xi, t) \sin n\eta$$

$$\phi = \frac{1}{2} H_0(\xi, t) + \sum_{n=1}^{N} H_n(\xi, t) \cos n\eta \qquad (10)$$

where N is the number of terms in the Fourier series.

Using the above expressions in equations (4), (5), and (6) results in the following set of differential equations for the unknown functions f_n, g_n, H_0 and H_n.

$$\cosh 2\xi \frac{\partial g_n}{\partial t} - \frac{1}{2}\left[\frac{\partial g_{(n+2)}}{\partial t} + \mathrm{sgn}\,(n-2)\frac{\partial g_{|n-2|}}{\partial t}\right]$$

$$= 2\lambda^2 Pr\left[\frac{\partial^2 g_n}{\partial \xi^2} - n^2 g_n\right] + S_n(\xi, t) \qquad (11)$$

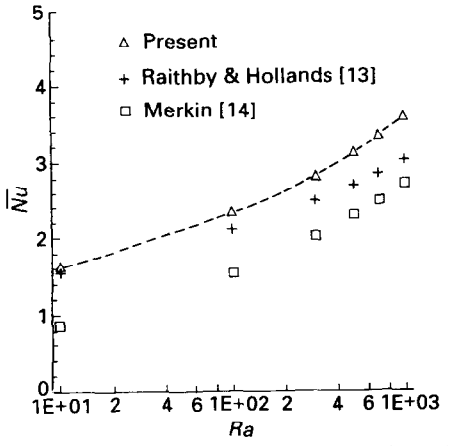

FIG. 3. Comparison of average Nusselt number for different Rayleigh numbers with previous theoretical results for the case of $b/a = 0.5$.

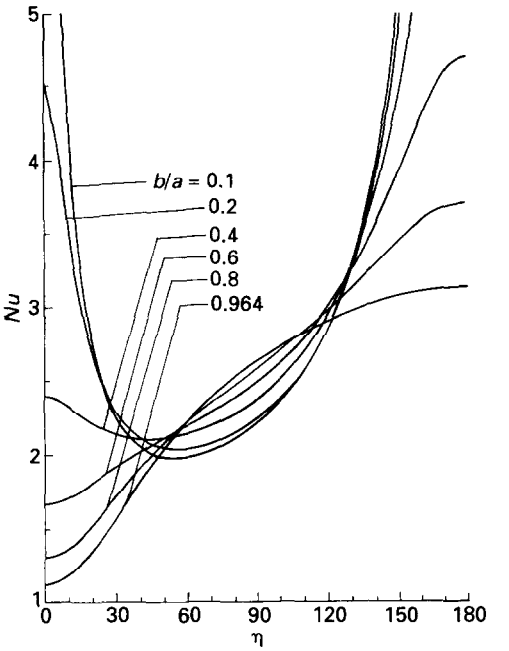

FIG. 4. Variation of the local Nusselt number with η for different axis ratios for the case of $Ra = 300$.

$$\frac{\partial^2 f_n}{\partial \xi^2} - n^2 f_n = -\frac{1}{2\lambda^2}$$

$$\times [\cosh 2\xi\, g_n - \tfrac{1}{2}(g_{(n+2)} + \mathrm{sgn}\,(n-2) g_{|n-2|})] \qquad (12)$$

$$\cosh 2\xi \frac{\partial H_0}{\partial t} - \frac{\partial H_2}{\partial t} = 2\lambda^2 \frac{\partial^2 H_0}{\partial \xi^2} - Z_n(\xi, t) \qquad (13)$$

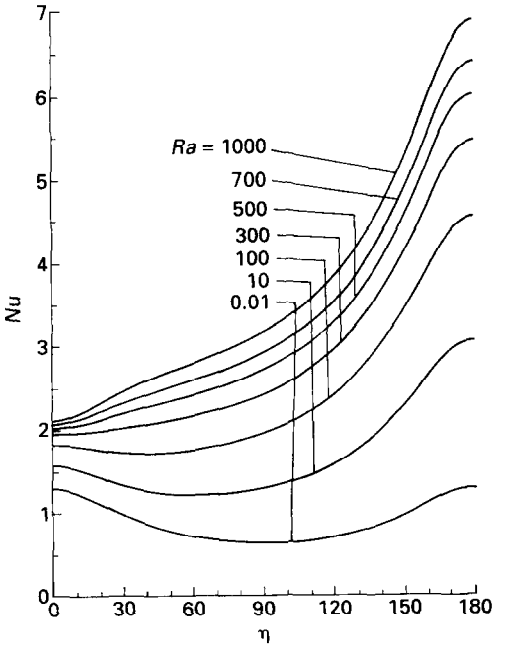

FIG. 5. Variation of the local Nusselt number with η for different Rayleigh numbers for the case of $b/a = 0.5$.

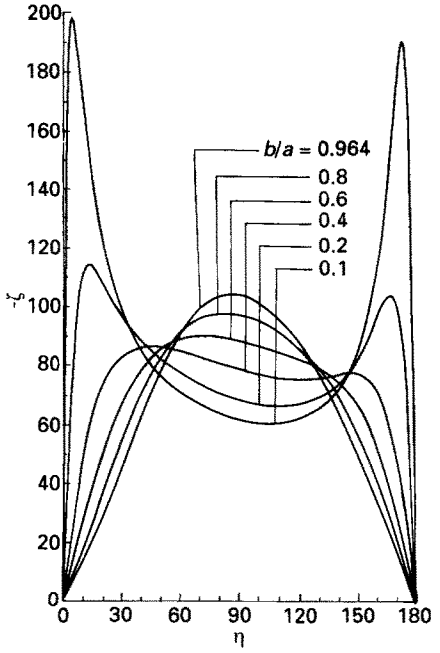

FIG. 6. Variation of the vorticity distribution with the cylinder surface for different axis ratios for the case of $Ra = 300$.

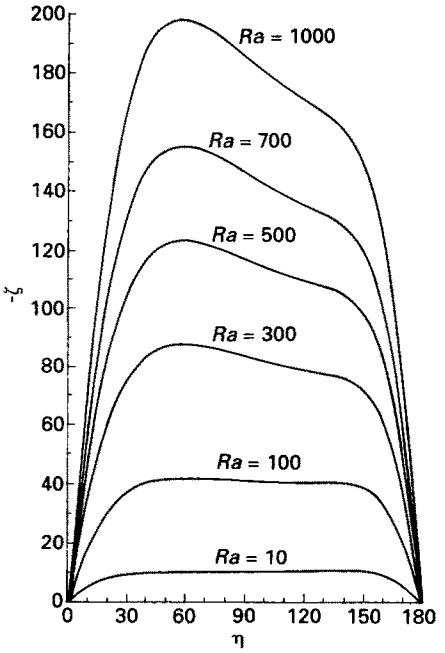

FIG. 7. Variation of the vorticity distribution on the cylinder surface for different Rayleigh numbers for the case of $b/a = 0.5$.

$$\cosh 2\xi \frac{\partial H_n}{\partial t} - \frac{1}{2}\left[\frac{\partial H_{(n+2)}}{\partial t} + \frac{\partial H_{|n-2|}}{\partial t}\right] = 2\lambda^2\left[\frac{\partial^2 H_n}{\partial \xi^2} - n^2 H_n\right] - Z_n(\xi, t) \quad (14)$$

where sgn $(n-2)$ means the sign of term $(n-2)$ and

$$\text{sgn}\,(n-2) = g_{|n-2|} = 0, \quad H_{|n-2|} = H_0 \quad \text{for} \quad n = 2.$$

The terms S_n, Z_0 and Z_n are known functions of ξ and t and are defined in the Appendix.

Equations (11)–(14) represent a set of partial differential equations in one space variable ξ instead of two space variables (ξ, η) in the original equations (4)–(6).

The use of Fourier series approximation satisfies the additional conditions given in equation (9) automatically. The boundary conditions stated in equation (8) may now be expressed in terms of the functions f_n, g_n, H_0 and H_n as

$$f_n = \frac{\partial f_n}{\partial \xi} = H_n = 0; \quad H_0 = 2 \quad \text{at} \quad \xi = \xi_0$$

$$\frac{1}{J^{1/2}} f_n, \quad \frac{1}{J^{1/2}} \frac{\partial f_n}{\partial \xi}, \quad g_n, \quad H_0, \quad H_n \to 0 \quad \text{as} \quad \xi \to \infty. \quad (15)$$

The boundary condition for the vorticity functions g_n at the cylinder surface $(\xi = \xi_0)$ is not easy to specify since it requires information about the velocity gradients which are not known a priori. To calculate these boundary value, integral conditions for g_n may be obtained following the work by Collins and Dennis [16]. By multiplying both sides of equation (12) by $e^{-n\xi}$ and then integrating from ξ_0 to ∞ subject to boundary conditions described in equation (15), one obtains:

$$\int_{\xi_0}^{\infty} e^{-n\xi}[\cosh 2\xi\, g_n - \tfrac{1}{2}\{g_{(n+2)} + \text{sgn}\,(n-2) g_{|n-2|}\}] = 0. \quad (16)$$

The values of the Fourier coefficients at the start of the solution $(t = 0)$ become

$$f_n(\xi, 0) = g_n(\xi, 0) = H_n(\xi, 0)$$

for

$$1 \leqslant n \leqslant N \quad \text{and} \quad \xi_0 \leqslant \xi \leqslant \infty$$

and

$$H_0(\xi, 0) = 0 \quad \text{for} \quad \xi > \xi_0$$

and

$$H_0(\xi, 0) = 2 \quad \text{for} \quad \xi = \xi_0. \quad (17)$$

The integration of equations (11)–(14) in time is carried out numerically. The numerical method is based on the Crank–Nicholson finite-difference scheme coupled with a form of predictor–corrector tech-

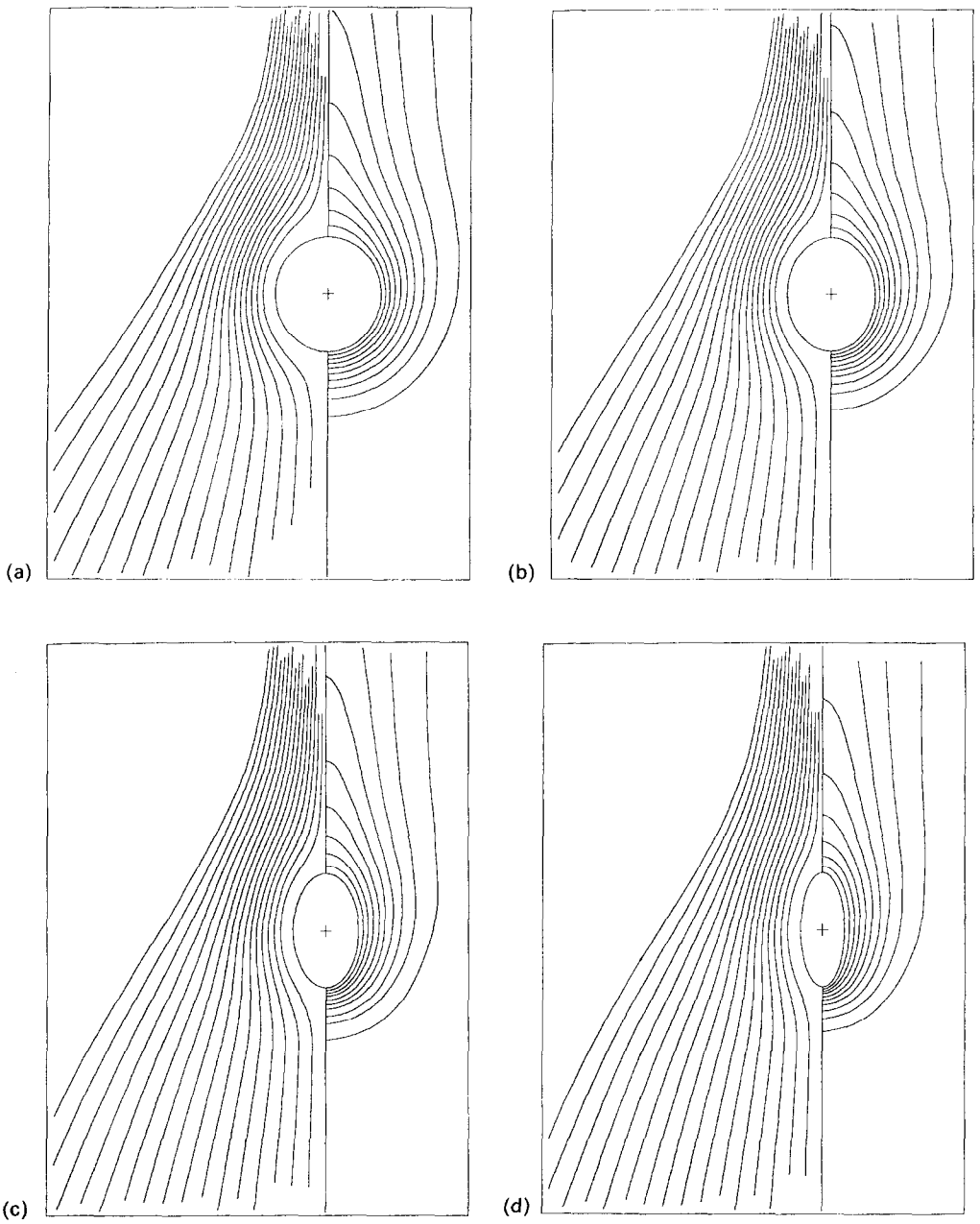

FIG. 8. Streamline and isotherm patterns for different axis ratios for the case of $Ra = 300$: (a) $b/a = 0.964$; (b) $b/a = 0.8$; (c) $b/a = 0.6$; (d) $b/a = 0.4$; (e) $b/a = 0.2$. Streamlines plotted are $\psi = 0.5, 1.0, \ldots, 8.0$ and isotherms plotted are $\phi = 0.1, 0.2, \ldots, 0.9$.

nique. The solution procedure is the same as that used by Badr [17] except for the unknown terms g_{n+2} and H_{n+2} in equations (11), (12), and (14) which were first approximated and then corrected through an iterative type procedure during every time step. The conditions at infinity are imposed at $\xi_{\max} = 10$ which corresponds to a very large distance from the cylinder surface (about 5000 times the major axis). At the start of computations, the number of terms in the Fourier series is taken as 7 and more terms are added as time increases until reaching the steady state. The maximum number of terms used is 20 in most of the cases considered. The logarithmic nature of the ξ coordinate enables us to have equal space steps in the discretization process while the physical space steps are very small near the solid boundary and large far away. Such discretization matches the physical phenomenon since the temperature and velocity gradients are large near the solid surface and become very small far away.

4. RESULTS AND DISCUSSION

Before presenting results let us first define the local and average Nusselt numbers (Nu, $\overline{Nu}$) as follows:

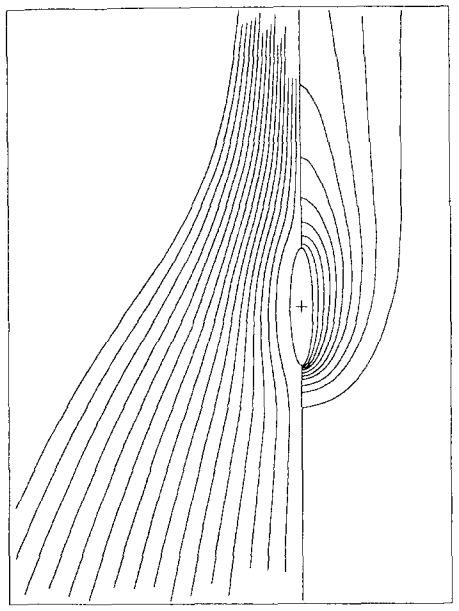

FIG. 8.—*Continued.*

$$Nu = \frac{bh}{k}, \quad \overline{Nu} = \frac{b\bar{h}}{k} \tag{18}$$

where k is the fluid thermal conductivity and h and $\bar{h}$ are the local and average heat transfer coefficient. These can be obtained from

$$h = \frac{\dot{q}}{T_s - T_\infty} = \frac{-k(\partial T/\partial S_n)_{\xi=\xi_0}}{T_s - T_\infty} \tag{19}$$

where $\dot{q}$ is the rate of heat transfer per unit area and S_n is the direction normal to the solid surface. Using the same coordinate transformation, equation (19) can be expressed in a dimensionless form as

$$h = -\frac{k}{J_0^{1/2}}\left(\frac{\partial \phi}{\partial \xi}\right)_{\xi=\xi_0} \tag{20}$$

where $J_0 = l^2/2(\cosh 2\xi_0 - \cos 2\eta)$ and the term $(\partial\phi/\partial\xi)_{\xi=\xi_0}$ can be expressed in terms of Fourier coefficients as

$$\left(\frac{\partial \phi}{\partial \xi}\right)_{\xi=\xi_0} = \frac{1}{2}\left(\frac{\partial H_0}{\partial \xi}\right)_{\xi=\xi_0} + \sum_{n=1}^{N}\left(\frac{\partial H_n}{\partial \xi}\right)_{\xi=\xi_0}.$$

Using the above expressions in equation (18) results in

$$Nu = \frac{-\sqrt{(2)}\lambda}{(\cosh 2\xi_0 - \cos 2\eta)^{1/2}}\left(\frac{\partial \phi}{\partial \xi}\right)_{\xi=\xi_0}. \tag{21}$$

The average Nusselt number may now be expressed as:

$$\overline{Nu} = \frac{1}{L}\int_0^L Nu\,\mathrm{d}L = -\frac{2\pi l \cosh\xi_0}{L}\left(\frac{\partial H_0}{\partial \xi}\right)_{\xi=\xi_0} \tag{22}$$

where L is the elliptical-section perimeter.

The effect of cylinder axis ratio on the average Nusselt number is shown in Fig. 2 for a constant Rayleigh number of 300. The available experimental and theoretical values of Nu for the two limiting cases of a vertical flate plate ($b/a = 0$) and a horizontal circular cylinder ($b/a = 1$) are also plotted on the same figure for comparison. The figure shows a difference of only 5% between the values of Nu obtained in this work for a thin elliptic cylinder of axis ratio 0.1 and the flat plate experimental results of Saunders [18]. The deviation from McAdams correlation is found to be 3.8% and a difference of 6.3% is found when comparing with the correlation of Churchill and Chu [19]. Such differences are quite acceptable considering the variations amongst various experimental results and correlations themselves. However, a large difference is found when comparing with the flat plate numerical results obtained by Suraino and Yang [20]. This large difference is believed to be due to the imposition of the far field boundary conditions in ref. [19] at a distance of only 2–3 times the plate length which greatly affected the flow behavior.

At the other end, when the elliptic cylinder geometry approaches a circular cylinder ($b/a = 0.964$), a difference of 2% is found when comparing with the correlation of McAdams [1] and almost the same difference with Morgan [11] while a difference of 15% is found when comparing with the correlation of Churchill and Chu [10]. The large difference in the later may be attributed to the use of a single correlation for a wide range of Ra.

The effect of Ra on the average Nusselt number for a fixed cylinder geometry ($b/a = 0.5$) is presented in Fig. 3 together with the conduction thickness correlation results of Raithby and Hollands [13] and the boundary-layer results obtained by Merkin [14]. The difference between the present results and the conduction thickness solution varies from 4 to 15% as the Rayleigh number increases from 10 to 1000. However, the difference between the present results and those obtained by Merkin [14] are unsurprisingly higher since the range of Ra considered in this work is far away from the range of applicability of any boundary-layer solution.

The effect of axis ratio on the local Nusselt number variation along the cylinder surface for a fixed value of Ra can be seen in Fig. 4. For the case of an axis ratio close to that of a circular cylinder ($b/a = 0.964$), the local value of Nu is highest at the forward stagnation point and decreases to a minimum at the rearmost point. The trend changes as the cylinder gets thinner. For axis ratios of 0.4 and below, the minimum value of Nu occurs between $\eta = 40°$ and $60°$ as shown in Fig. 4. Although the average Nusselt numbers change only very slightly from $b/a = 0$ to $b/a = 1$ (Fig. 2), the local Nusselt number distributions (Fig. 4) are very different. The effect of Rayleigh number on the local Nusselt number distribution is shown in Fig. 5 for a fixed axis ratio of 0.5. The figure shows that for very small Ra values ($Ra = 0.01$) the local Nu distribution is almost symmetric about $\eta = 90°$ with

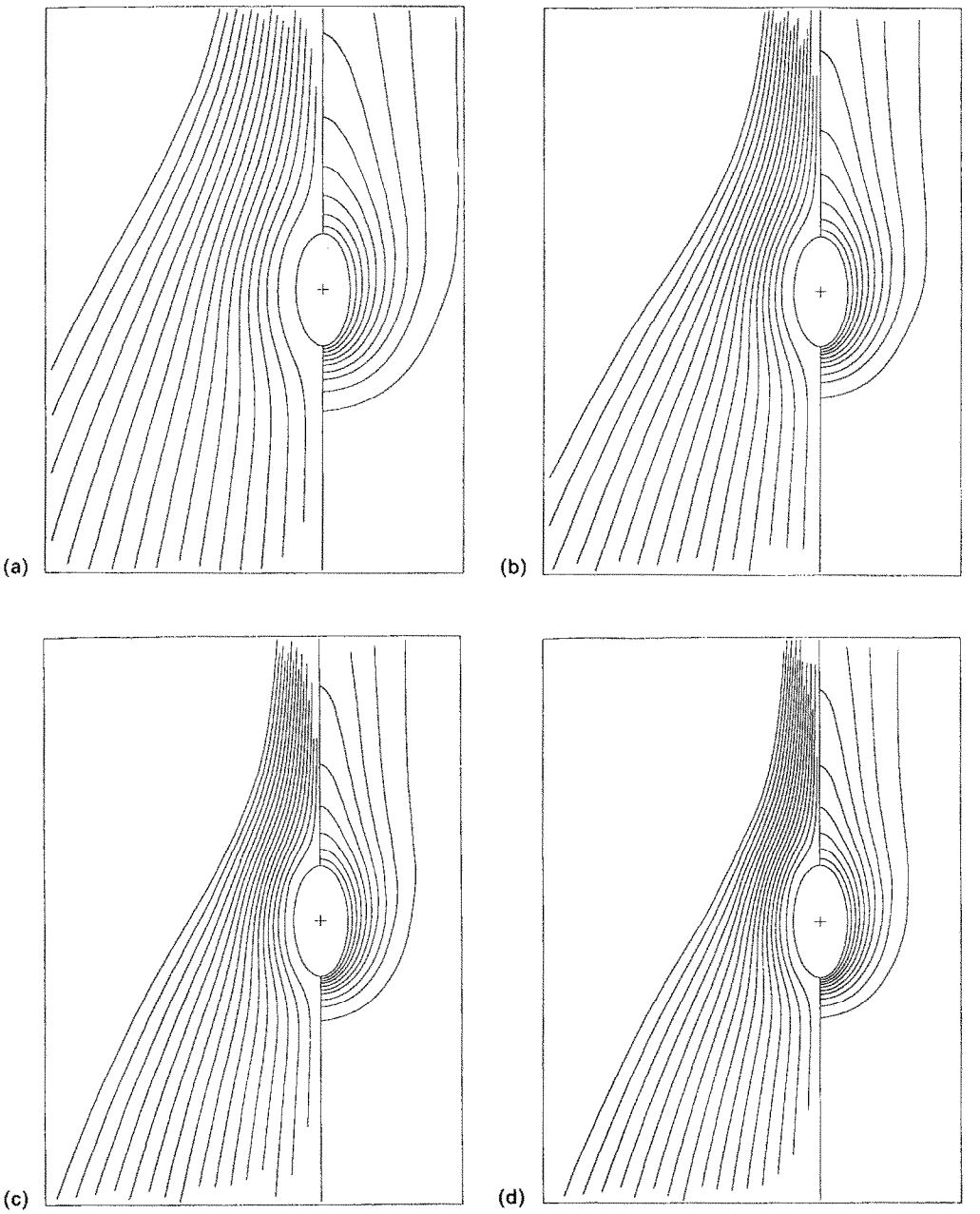

FIG. 9. Streamline and isotherm patterns for different Rayleigh numbers for the case of $b/a = 0.5$: (a) $Ra = 100$; (b) $Ra = 300$; (c) $Ra = 500$; (d) $Ra = 700$; (e) $Ra = 1000$. Streamlines and isotherms plotted are the same as in Fig. 8.

maximum values at both forward and backward stagnation points indicating a dominant conduction regime. The effect of increasing Ra is simply to increase the value of Nu over the entire cylinder surface with a larger increase at the forward stagnation point than at the rearward point. This shows that convection becomes more dominant with the increase of Ra.

The vorticity variation over the cylinder surface is shown in Fig. 6 for a Rayleigh number of 300 and different axis ratios. For an axis ratio of 0.964, the vorticity distribution is almost symmetric about $\eta = 90°$ and has its peak there. However, the asymmetry grows with the decrease of b/a and the maximum vorticity point shifts towards $\eta = 0°$ with another peak near $\eta = 180°$. As the cylinder gets thinner, the surface vorticity reaches very high values near $\eta = 0°$ and 180° but with no flow separation anywhere on the surface in all cases. The effect of increasing Ra on the surface vorticity is presented in Fig. 7 for an axis ratio of 0.5. At very small values of Ra, the surface vorticity is small and almost symmetric about $\eta = 90°$ (similar to the local Nu distribution). With the increase of Ra the vorticity increases over

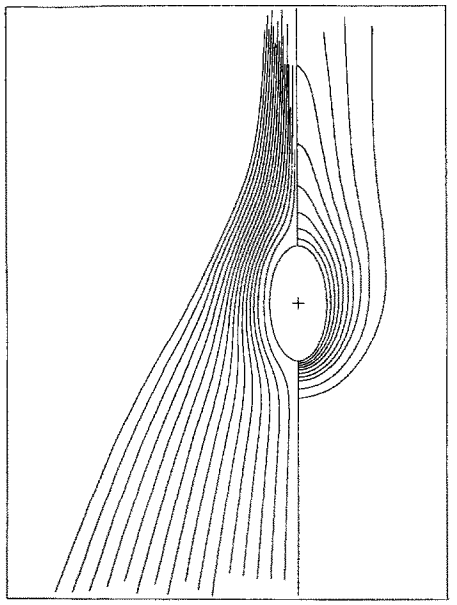

FIG. 9.—*Continued.*

the entire cylinder surface and it no longer remains symmetric.

The effect of axis ratio on the isotherm and streamline patterns for the case of $Ra = 300$ when $b/a = 0.964$, 0.8, 0.6, 0.4, and 0.2 is shown in Fig. 8. Since the velocity and thermal fields are symmetric about the line $\eta = 0°$, only one half of the field is plotted. The figure shows that the isotherms get closer to the body surface as the cylinder gets thinner. For the case of $b/a = 0.964$, the isotherm pattern (Fig. 8(a)) indicates a maximum temperature gradient at the bottom of the body ($\eta = 180°$) and a minimum at the top ($\eta = 0°$). However, for smaller axis ratios the temperature gradient possesses two peaks, one at the top of the body and the other at the bottom. The streamline patterns show that the fluid is accelerating from a low velocity region below the cylinder to a high velocity region above it. This is quite expected as a result of the buoyancy forces.

The isotherm and streamline patterns for Rayleigh numbers of 100, 300, 500, 700, 1000 when the cylinder axis ratio is 0.5 are plotted in Fig. 9. The figure shows higher stream velocities in the entire flow domain as Ra increases. The isotherm patterns show that the thermal layer gets thinner indicating higher temperature gradient as Ra increases.

5. CONCLUSIONS

The problem of free convection heat transfer from an isothermal elliptic cylinder is studied in the range $10 < Ra < 1000$ for axis ratios between 0.1 and 0.964. The method of solution is verified by comparing the average Nusselt number results with the available theoretical and experimental data for the circular cylinder and flat plate as two limiting cases and a good agreement is found. For a constant Rayleigh number, the average Nusselt number is found to increase with the decrease of the axis ratio approaching its maximum when the axis ratio approaches zero. The average and local heat transfer coefficients are also found to increase with the increase of Ra due to the increase of flow velocity. A similar behavior is also found for the surface vorticity. The local Nusselt number reaches high values at the forward and backward stagnation points as the cylinder gets thinner. The surface vorticity distribution indicated no flow separation anywhere on the cylinder surface. The obtained values of the local and average Nusselt numbers are believed to fill a gap in the existing knowledge about such problem.

Acknowledgements—The authors wish to acknowledge the support received from King Fahd University of Petroleum & Minerals during the course of this study. The valuable comments of one of the referees are greatly appreciated.

REFERENCES

1. W. H. McAdams, *Heat Transmission*. McGraw-Hill, New York (1954).
2. R. Hermann, Heat transfer by free convection from horizontal cylinders in diatomic gases, NACA TM 1366 (1954).
3. T. Chiang and J. Kay, On laminar free convection from a horizontal cylinder, *Proceedings of 4th National Congress of Applied Mechanics*, pp. 1213–1219 (1962).
4. L. Elliot, Free convection on a two-dimensional or axisymmetric body, *Q. J. Mech. Appl. Math.* **23**, 153–162 (1970).
5. J. H. Merkin, Free convection on an isothermal horizontal cylinder, ASME Paper No. 76-HT-16 (1976).
6. L. Pera and B. Gebhart, Experimental observations of wake formation over cylindrical surfaces in natural convection flows, *Int. J. Heat Mass Transfer* **15**, 175–177 (1972).
7. T. H. Kuehn and R. J. Goldstein, Numerical solution to the Navier–Stokes equations for laminar natural convection about a horizontal isothermal circular cylinder, *Int. J. Heat Mass Transfer* **23**, 971–979 (1980).
8. B. Farouk and S. I. Guceri, Natural convection from a horizontal cylinder—laminar regime, *ASME J. Heat Transfer* **103**, 522–527 (1981).
9. H. M. Badr, Heat transfer in transient buoyancy driven flow adjacent to a horizontal rod, *Int. J. Heat Mass Transfer* **30**, 1997–2012 (1987).
10. S. W. Churchill and H. S. Chu, Correlating equations for laminar and turbulent free convection from a horizontal cylinder, *Int. J. Heat Mass Transfer* **18**, 1049–1053 (1975).
11. T. V. Morgan, The overall convective heat transfer from smooth circular cylinders. In *Advances in Heat Transfer*, Vol. 4, pp. 199–264. Academic Press, New York.
12. F. N. Lin and B. T. Chao, Laminar free convection over two-dimensional and axisymmetric bodies of arbitrary contour, *ASME J. Heat Transfer* **96**, 435–442 (1974).
13. G. D. Raithby and K. G. T. Hollands, Laminar and turbulent free convection from elliptic cylinders, with a vertical plate and horizontal circular cylinder as special cases, *ASME J. Heat Transfer* **98**, 72–80 (1976).
14. J. H. Merkin, Free convection boundary layers on cylinders of elliptic cross-section, *ASME J. Heat Transfer* **99**, 453–457 (1977).

15. H. M. Badr, Laminar combined convection from a horizontal cylinder—parallel and contra flow regimes, *Int. J. Heat Mass Transfer* **27,** 15–27 (1984).
16. W. M. Collins and S. C. R. Dennis, Flow past an impulsively started circular cylinder, *J. Fluid Mech.* **60,** 105–127 (1973).
17. H. M. Badr, A theoretical study of laminar mixed convection from a horizontal cylinder in a cross stream, *Int. J. Heat Mass Transfer* **26,** 639–653 (1983).
18. O. A. Saunders, The effect of pressure on natural convection in air, *Proc. R. Soc. Lond, Series A* **157,** 278–291 (1936).
19. S. W. Churchill and H. S. Chu, Correlating equations for laminar and turbulent free convection from a vertical plate, *Int. J. Heat Mass Transfer* **18,** 1323–1329 (1975).
20. F. J. Suriano and K. T. Yang, Laminar free convection about vertical and horizontal plates at small and moderate Grashof numbers, *Int. J. Heat Mass Transfer* **11,** 473–490 (1968).

APPENDIX

The functions S_n, Z_0 and Z_n used in equations (25), (27) and (28) respectively, are as follows:

$$S_n(\xi,t) - \lambda\, Ra\, Pr\left[\cosh\xi\left\{\frac{\partial H_{(n+1)}}{\partial\xi} - \frac{\partial H_{(n-1)}}{\partial\xi}\right\} + \sinh\xi\{(n+1)H_{(n+1)} + (n-1)H_{|n-1|}\}\right] + \lambda^2\sum_{m=1}^{N}\left[\frac{\partial g_m}{\partial\xi}\{(m+n)f_{(m+n)} - |m-n|f_{|m-n|}\} + mg_m\left\{\frac{\partial f_{(m+n)}}{\partial\xi} - \operatorname{sgn}(m-n)\frac{\partial_{|m-n|}}{\partial\xi}\right\}\right] \tag{A.1}$$

$$Z_0(\xi,t) = 2\lambda^2\sum_{m=1}^{N} m\left\{f_m\frac{\partial H_m}{\partial\xi} + H_m\frac{\partial f_m}{\partial\xi}\right\} \tag{A.2}$$

$$Z_n(\xi,t) = \lambda^2 n f_n\frac{\partial H_0}{\partial\xi} + \lambda^2\sum_{m=1}^{N}\left[\frac{\partial H_m}{\partial\xi}\{(m+n)f_{(m+n)} + |m-n|f_{|m-n|}\} + mH_m\left\{\frac{\partial f_{(m+n)}}{\partial\xi} + \operatorname{sgn}(m-n)\frac{\partial f_{|m-n|}}{\partial\xi}\right\}\right] \tag{A.3}$$

where sgn $(m-n)$ represents the sign of the term $(m-n)$ and $f_0 = g_0 = 0$.